ACS APPLIED MATERIALS & INTERFACES

Research Article

www.acsami.org

Enhancement of the Electron Field Emission Properties of Ultrananocrystalline Diamond Films via Hydrogen Post-Treatment

Kamatchi Jothiramalingam Sankaran,[†] Srinivasu Kunuku,[‡] Keh-Chyang Leou,[‡] Nyan-Hwa Tai,*[,†] and I-Nan Lin*[,§]

[†]Department of Materials Science and Engineering and [‡]Department of Engineering and System Science, National Tsing Hua University, Hsinchu 300, Taiwan, Republic of China

[§]Department of Physics, Tamkang University, Tamsui 251, Taiwan, Republic of China

ABSTRACT: Enhanced electron field emission (EFE) properties due to hydrogen post-treatment at 600 °C have been observed for ultrananocrystalline diamond (UNCD) films. The EFE properties of H_2-gas-treated UNCD films could be turned on at a low field of 5.3 V/μm, obtaining an EFE current density of 3.6 mA/cm^2 at an applied field of 11.7 V/μm that is superior to those of UNCD films treated with H_2 plasma. Transmission electron microscopic investigations revealed that H_2 plasma treatment induced amorphous carbon (a-C) (and graphitic) phases only on the surface region of the UNCD films but the interior region of the UNCD films still contained very small amounts of a-C (and graphitic) grain boundary phases, resulting in a resistive transport path and inferior EFE properties. On the other hand, H_2 gas treatment induces *a*-C (and graphitic) phases along the grain boundary throughout the thickness of the UNCD films, resulting in creation of conduction channels for the electrons to transport from the bottom of the films to the top and hence the superior EFE properties.

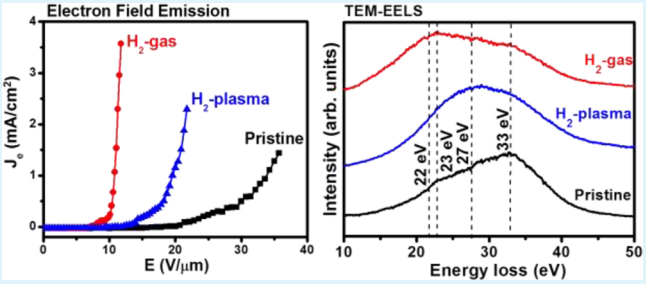

KEYWORDS: *ultrananocrystalline diamond films, hydrogen post-treatments, electron field emission, plasma illumination, electron energy loss spectroscopy*

INTRODUCTION

Diamond and related materials have enormous prospective applications due to their excellent physical and chemical properties.[1,2] Among diamond films with various granular structures, the ultrananocrystalline diamond (UNCD) film is a more promising material due to its unique and advantageous properties similar to those of conventional microcrystalline and nanocrystalline diamond films, such as high hardness and smoothness, chemical inertness, negative electron affinity (NEA) characteristics, high transmittance in the near-infrared region, and the likelihood of p- and n-type conductivities by doping.[3−6] The UNCD films are superior to conventional diamond films in many ways, which widespread research has confirmed. Moreover, nanosizing of diamond crystals increases the grain boundaries, containing nondiamond carbons, in the UNCD films and has been observed to markedly enhance the electron field emission (EFE) properties of the films.[7,8] UNCD films with ultrasmall grain sizes of 5−10 nm and sp^2-rich grain boundaries show better EFE characteristics as compared to the conventional diamond films.[9] Consequently, UNCD films possess better potential application for cold cathode field emitters and vacuum nanoelectronic devices. Appropriate modification and control of microstructures of UNCD films can modify their physical and chemical properties for emerging new applications and technologies. Prior studies have reported that a proper increase in amorphous carbon (a-C) and graphitic phase grain boundaries[10,11] would form possible interconnected paths for facilitating the transport of electrons and markedly enhance the EFE properties.

In addition, the modification of surface characteristics of diamond films plays an important role in enhancing the EFE behavior of the films. The EFE properties of diamond films were markedly altered when coated with wide-band-gap materials.[12] Even when the surface of a diamond film is bonded with different species, the band structure below the surface is altered, which changes the EFE properties. The type of surface treatment influences the surface conductivity and electron affinity properties. For example, hydrogen treatment of diamond shows p-type surface conductivity with NEA,[13,14] whereas oxygen treatment of diamond induced surface-insulating properties with a positive electron affinity.[15,16] The change of surface treatment of diamond (O_2 or H_2) is reversible and controllable, which has created a niche application for diamond in sensors, biology, and electronics applications.[17−19] The hydrogen treatment is of particular interesting owing to its simplicity and versatility. Hydrogen treatment of diamond usually has been achieved using atomic hydrogen produced by either plasma or hot filament techniques[20,21] and was lately also

Received: June 16, 2014
Accepted: August 5, 2014
Published: August 5, 2014

done electrochemically.[22] Manfredotti et al. observed that the thermal hydrogenation can give rise to a surface conducting layer with the same electrical characteristics observed in plasma hydrogenation.[23] Ando et al. demonstrated the possibility of thermal hydrogen by exposing diamond powders to a pure molecular hydrogen flow in the temperature range of 400–1100 °C.[24] Fizzotti et al. reported that thermal hydrogenation of diamond using molecular hydrogen on single-crystal diamond at 800 °C gave rise to surface conduction and was interpreted through the electrochemical transfer-doping model.[25] Particularly, enhancement of the EFE properties was observed for the surface-treated UNCD films.[26−28] However, these reports on the effect of H_2 post-treatment of the electrical conductivity/EFE properties of the diamond films are controversial, and the mechanism by which the H_2 post-treatment process influenced the EFE properties of these films has not been fully understood yet.

In this study, the UNCD films were subjected to two different hydrogen post-treatments: (1) hydrogen plasma treatment of the UNCD films was performed in a microwave plasma enhanced chemical vapor deposition (MPECVD) system, and (2) hydrogen gas treatment was carried out by placing the UNCD films in a nonplasma quartz tube reactor connected with a H_2 gas supply line at low treatment temperature. We observed a significant effect of these two post-treatment processes on enhancing the plasma illumination (PI) and the EFE properties of the UNCD films. The modifications to the bonding structure of these films due to these hydrogen post-treatment processes were investigated in detail by electron energy loss spectroscopy (EELS) in transmission electron microscopy (TEM). A possible mechanism for the enhancement of EFE and PI properties of UNCD films is discussed.

EXPERIMENTAL METHODS

The UNCD films were grown on n-type mirror polished Si substrates in an MPECVD (2.45 GHz 6 in. IPLAS-CYRANNUS-I, Troisdorf, Germany) system. Prior to the deposition of UNCD films, the silicon substrates were preseeded by ultrasonication in methanol solution, containing nanosized diamond powders (~5 nm) and Ti powders (~32.5 nm) for 45 min. The substrates were ultrasonicated again in methanol for 1 min to remove the possibly adhered nanoparticles. The UNCD films were grown in Ar (99%)/CH_4 (1%) plasma (100 sccm) at a microwave power of 1200 W and at a pressure of 120 Torr (16 kPa) for 5 h, without the substrate being heated. The substrate was heated due to the bombardment of the plasma species, and the substrate temperature was estimated to be around 475 °C during the growth of the UNCD films. The pristine UNCD films were subjected to two different hydrogen post-treatment processes. In the first method, the pristine UNCD films were H_2-plasma-treated in the same IPLAS-CYRANNUS-I MPECVD system for 5 min at a microwave power of 600 W, a pressure of 5 Torr (666 Pa) (with 100 sccm of H_2 flow), and a temperature of 600 °C. Thus, the obtained samples are designated as "H_2-plasma-treated UNCD" films. In the other process, the UNCD films were thermally heat-treated in a H_2 environment; i.e., the UNCD films were heated in a nonplasma quartz tube reactor to 600 °C under H_2 gas (99.999% pure flow, 20 sccm) for 2 h, followed by cooling to room temperature under a continuous H_2 gas flow. Thus, the obtained samples are designated as "H_2-gas-treated UNCD" films.

The films were characterized using field emission scanning electron microscopy (FESEM; Jeol 6500), atomic force microscopy (AFM; Smena-B, NT-MDT, Russia), and visible-Raman spectroscopy (λ = 632.8 nm, spectral resolution 0.5 cm^{-1}, Lab Raman HR800, Jobin Yvon). The detailed microstructure and bonding structure of the samples were examined using EELS (Gatan Enfina) in TEM (Jeol 2100F). The electrical resistivity of the UNCD films was measured by a four-probe technique, in which two configurations were utilized: (i) with all four probes located on the surface of the films for measuring the resistivity along the film surface and (ii) with two of the probes located on the UNCD film surface and the other two probes located on the UNCD-to-Si interface for measuring the resistivity through the film thickness. The EFE properties of the UNCD films were measured with a tunable parallel-plate setup, in which the cathode-to-anode distance was controlled using a micrometer. The current density–applied field (J_e–E) characteristics were measured using an electrometer (Keithley 2410) under a pressure below 10^{-6} Torr (1.3×10^{-4} Pa). The EFE behavior of the materials was modeled with the Fowler–Nordheim (F–N) theory.[29] The turn-on field (E_0) was designated as the point of interception of the straight lines extrapolated from the low- and high-field segments of the F–N plots, namely, $\log(J_e/E^2)$ versus $1/E$ plots.

The PI characteristics of a microcavity were also investigated, in which an indium tin oxide (ITO)-coated glass was used as the anode and the UNCD films were used as the cathode. The cathode-to-anode separation was fixed by a poly(tetrafluoroethylene) (PTFE) spacer (1.0 mm in thickness). A circular hole about 6.0 mm in diameter was cut from the spacer (PTFE) to shape a microcavity. The chamber was evacuated to reach a base pressure of 0.1 mTorr (13 mPa) and then purged with Ar for 10 min. The Ar gas was flowed into the chamber at a flow rate of 10 sccm throughout the measurements. The plasma was triggered using a pulsed direct current voltage in a bipolar pulse mode (20 ms square pulse, 6 kHz repetition rate) at 12 Torr (1599 Pa). The plasma current versus applied voltage behavior was measured using an electrometer (Keithley 237).

RESULTS AND DISCUSSION

Figure 1 shows the apparent changes in the morphology of the films due to hydrogen treatments. The pristine UNCD films

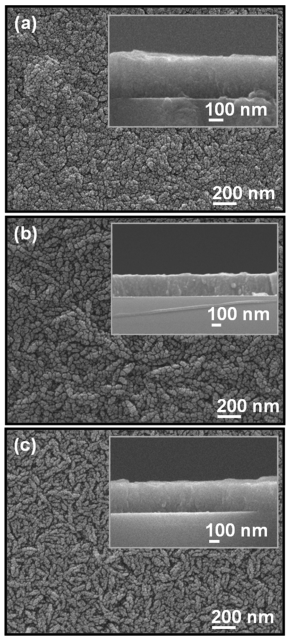

Figure 1. FESEM images of (a) pristine, (b) H_2-plasma-treated, and (c) H_2-gas-treated UNCD films. The insets show the corresponding cross-sectional FESEM images.

contain random and spherically structured grains (Figure 1a). The thickness of the pristine UNCD was about 400 nm, which was estimated from a cross-sectional FESEM image (inset, Figure 1a). The root-mean-square (rms) roughness of the pristine UNCD films was 7.8 nm, which was estimated using AFM (figure not shown). More distinct and clear grains and

grain boundaries were observed after 5 min of H_2 plasma treatment due to etching of nondiamond carbon from the surface of the UNCD films (Figure 1b). The thickness (inset, Figure 1b) and the rms roughness (figure not shown) of the H_2-plasma-treated UNCD films were reduced to 350 and 6.7 nm. Agglomeration of the nanosized grains was induced for the UNCD films post-treated in H_2 gas, resulting in the elongated granular morphology (Figure 1c). The thickness of the films was reduced to around 380 nm (inset, Figure 1c), and the rms roughness was estimated to be 8.9 nm. It seems that both the H_2 plasma and H_2 gas post-treatment processes resulted in some etching on the surface of the diamond films.

Figure 2 depicts the visible−Raman spectra of (I) pristine, (II) H_2-plasma-treated, and (III) H_2-gas-treated UNCD films.

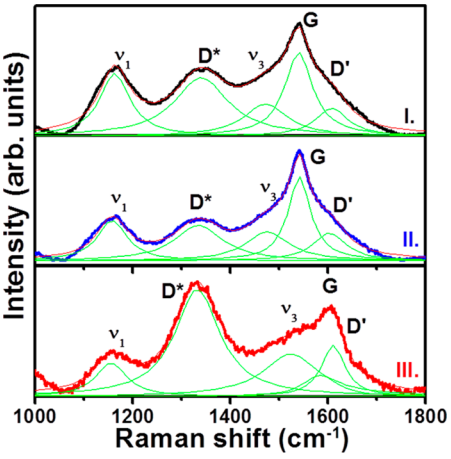

Figure 2. Visible−Raman spectra from (I) pristine, (II) H_2-plasma-treated, and (III) H_2-gas-treated UNCD films taken at 632.8 nm.

The Raman spectra were deconvoluted by using teh multipeak Lorentzian fitting method. Peaks at around 1160 and 1470 cm^{-1} are attributed to the ν_1 and ν_3 modes of *trans*-polyacetylene (*t*-PA) present in the grain boundaries of pristine UNCD films (curve I, Figure 2).[30] A broadened peak around 1340 cm^{-1} (designated as the D* band), which correlates to the disordered sp^2-bonded carbon, is observed for the films.[31] The sharp Raman peak at 1332 cm^{-1} corresponding to the F_{2g} zone center optical phonon of diamond is not clearly observable in this Raman spectrum as visible−Raman spectroscopy is overwhelmingly more sensitive to sp^2 sites. The G band of the UNCD film is observed at around 1540 cm^{-1}. A shoulder peak around 1607 cm^{-1} (designated as the D′ band) is seen, which possibly arises from the nanocrystalline graphitic content in the films.[32] Curves II and III of Figure 2 show the effect of H_2 post-treatments on altering the bonding characteristics of the UNCD films. They show higher intensities of the D* and G peaks, indicating amorphization and graphitization types of transitions.[33] Particularly, the ν_3 peak of H_2-gas-treated UNCD films is not clearly observed as it merged with the G band due to the use of a red laser, as can be seen in curve III of Figure 2. Interestingly, there is a big shift in the G and ν_3 peaks for H_2-gas-treated UNCD films, indicating that the increase in a-C (or graphite) phases of the H_2-gas-treated UNCD films is higher as compared to that of the H_2-plasma-treated UNCD films.[34] However, the change in Raman structure cannot unambiguously differentiate the effect of H_2 plasma and H_2 gas treatment processes on altering the characteristics of UNCD films. A more detailed investigation on the microstructure/bonding structure of these films using TEM/EELS is necessary, which will be discussed shortly.

The electrical resistivity of the UNCD films was measured by the four-probe technique. Figure 3a indicates the resistivity

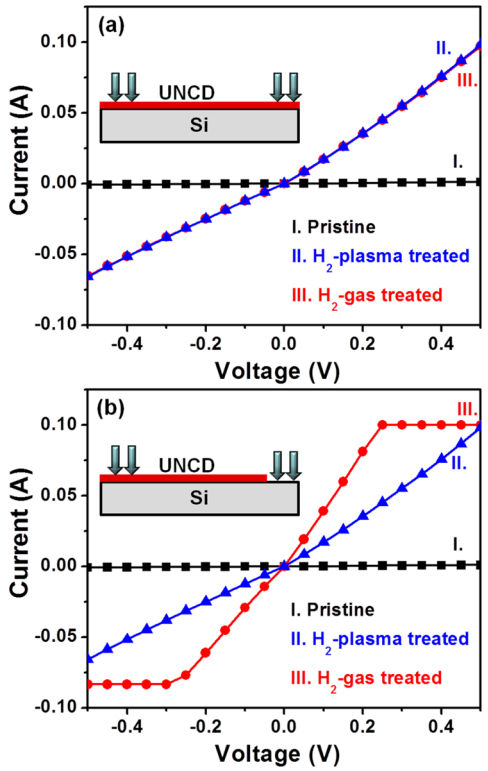

Figure 3. Electrical resistivity (current−voltage curves) measured by the four-probe technique for (I) pristine, (II) H_2-plasma-treated, and (III) H_2-gas-treated UNCD films. The current was flowing either (a) along the surface of the films (i.e., with all four probes on the same surface of the films, inset) or (b) across the films (i.e., with two of the probes on the surface of the diamond films and two on the Si substrates, inset).

along the UNCD film surface (ρ_s), whereas Figure 3b shows the resistivity through the film thickness (ρ_t). The configurations for measuring ρ_s and ρ_t are shown in the respective insets. This figure indicates that both the H_2-post-treated UNCD films show markedly better conductivity compared to the pristine UNCD films. Figure 3a reveals that the surface resistivity (ρ_s) is very large (0.15 Ω cm, curve I of Figure 3a) for pristine UNCD films. The H_2 plasma and H_2 gas treatment processes markedly lowered the surface resistivity of the UNCD films. The ρ_s value of the H_2-plasma-treated UNCD (0.022 Ω cm) is similar to those of the H_2-gas-treated UNCD films (0.024 Ω cm) (curves II and III, Figure 3a). In contrast, Figure 3b shows the through-film resistivity (ρ_t) is around 0.46 × 10^{-4} Ω cm for the H_2-gas-treated UNCD films (curve III, Figure 3b), which is noticeably smaller than the ρ_t value for H_2-plasma-treated UNCD films (1.15 × 10^{-3} Ω cm, curve II of Figure 3b). The pristine UNCD films show markedly larger through-film resistivity (2.68 × 10^{-2} Ω cm, curve I of Figure 3b). These resistivity values with the percentage of error in measurements are listed in Table 1.

Figure 4a shows the EFE properties of these UNCD films, with the inset showing the corresponding F−N plots. As seen from the J_e versus E curves, the EFE properties are significantly enhanced due to the H_2 post-treatment processes (curves II

Table 1. Electrical Resistivity (Current−Voltage Curves) Measured by the Four-Probe Technique, Electron Field Emission, and Plasma Illumination Properties of UNCD Films That Have Undergone Different Hydrogen Treatments[a]

	four-probe measurements		electron field emission			plasma illumination	
UNCD film	ρ_t (Ω cm) (error, %)	ρ_s (Ω cm) (error, %)	E_0 (V/μm) (error, %)	J_e (mA/cm^2) (error, %)	E_{th} (V/μm) (error, %)	J_{pl} (mA/cm^2) at 0.55 V/μm (error, %)	n_e (/cm^3) at 5000 V/cm (error, %)
pristine	2.68×10^{-2} (3.5)	0.15 (7.5)	18.5 (7.8)	1.4 (8.0) at 35.7 V/μm	0.35 (4.5)	0.47 (5.6)	1.87×10^{16} (5.8)
H_2-plasma-treated	1.15×10^{-3} (9.1)	0.022 (8.9)	10.4 (8.9)	2.3 (9.2) at 21.8 V/μm	0.33 (6.3)	0.50 (6.2)	2.10×10^{16} (6.2)
H_2-gas-treated	0.46×10^{-4} (6.2)	0.024 (4.9)	5.3 (4.9)	3.6 (7.5) at 11.7 V/μm	0.31 (7.5)	0.54 (6.8)	2.46×10^{16} (7.1)

[a] ρ_t is the through-film resistivity measured using two probes placed on the UNCD surface and the other two probes on the UNCD-to-Si interface. ρ_s is the surface resistivity measured using all four probes placed on the UNCD surface. E_0 is the turn-on field for the EFE process that was designated as the interception of the lines extrapolated from the high-field and low-field segments of the F−N plots. J_e is the EFE current density evaluated at the applied field designated. E_{th} is the threshold field needed to trigger the plasma for the microplasma devices. J_{pl} is the plasma current density at 0.55 V/μm applied field for the microplasma devices. n_e is the plasma density estimated from the plasma current density at 5000 V/cm applied field for the microplasma devices.

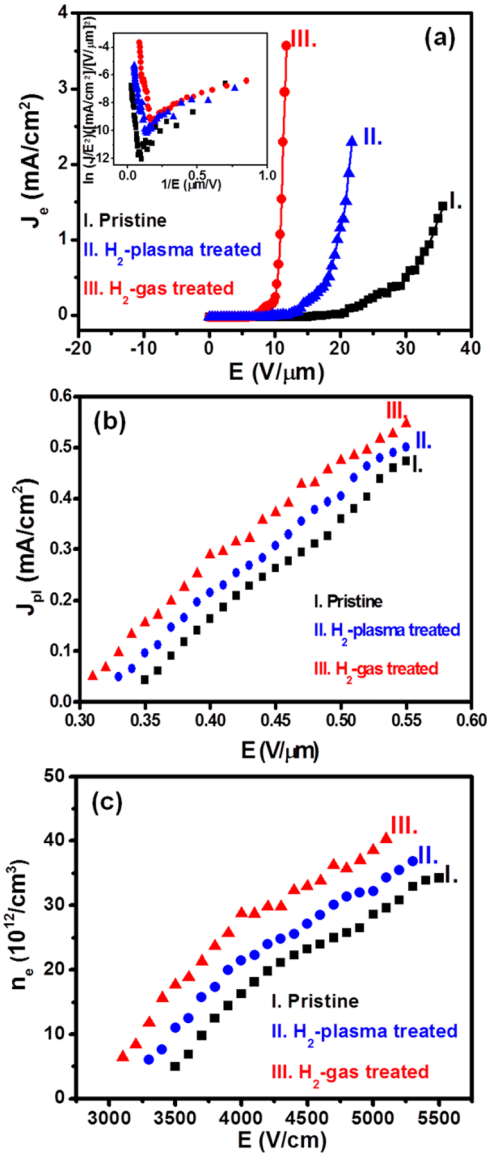

Figure 4. (a) Electron field emission (with corresponding F−N plots shown as an inset), (b) plasma current density against applied field curves, and (c) plasma density against applied field curves of (I) pristine, (II) H_2-plasma-treated, and (III) H_2-gas-treated UNCD films.

and III, Figure 4a), as compared to those of pristine UNCD films (curve I, Figure 4a). Better EFE properties are observed for H_2-gas-treated UNCD films compared to H_2-plasma-treated UNCD films. The E_0 value was lowered from 18.5 V/μm for pristine UNCD films to 5.3 V/μm for H_2-gas-treated UNCD films. A better J_e value of 3.6 mA/cm^2 at an applied field (E_a) of 11.7 V/μm is obtained for H_2-gas-treated UNCD films (curve III, Figure 4a), whereas the J_e value for pristine UNCD films is markedly smaller, i.e., J_e = 1.4 mA/cm^2, at E_a = 35.7 V/μm. These vaules are given in Table 1, including the percentage of error in the measurements. In contrast, for H_2-plasma-treated UNCD films (curve II, Figure 4a), the E_0 value is 10.4 V/μm and the J_e value is 2.3 mA/cm^2 at E_a = 21.8 V/μm, and these values are markedly better than those for the pristine UNCD films but are still inferior to those for the H_2-gas-treated UNCD films. The comparison of the EFE properties of H_2-gas-treated UNCD films with those of other plasma-treated electron field emitting materials is summarized in Table 2.[35−38] The

Table 2. Comparison of Electron Field Emission Properties of H_2-Gas-Treated UNCD Films with Those of Various Plasma-Treated Electron Field Emitting Materials

electron field emitting material	E_0 (V/μm)	J_e (mA/cm^2)
H_2-plama-treated diamond nanowires[28]	4.2	5.1 at 8.5 V/μm
H_2-plasma-treated tungsten oxide nanowires[35]	4.7	0.15 at 6.0 V/μm
H_2-plasma-treated ZnO films[36]	3.6	16.0 at 1.3 V/μm
Ar-plasma-treated ultrasharp α-Fe_2O_3 nanoflakes[37]	8.0	0.06 at 11.0 V/μm
H_2-plasma-treated diamond-like carbon[38]	1000	
H_2-gas-treated UNCD films (present study)	5.3	3.6 at 11.7 V/μm

enhancement in EFE properties is closely related to the improvement in the electrical conductivity of the films. Restated, both the better surface and bulk electrical characteristics of the H_2-gas-treated UNCD films distinctly improved the EFE properties.

On the other hand, Figure 5 shows a series of photographs of the PI behavior of the microplasma devices, which utilized the UNCD films as cathode materials. The intensity of the plasma illumination increases monotonically with the applied voltage. These figures show that the devices using H_2-gas-treated UNCD films as cathodes (Figure 5c) exhibit superior illumination behavior compared to those using pristine and

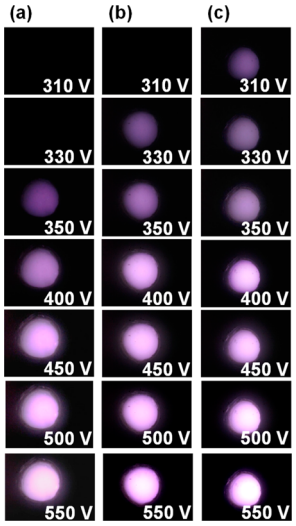

Figure 5. Plasma illumination characteristics for the microplasma devices utilizing (a) pristine, (b) H_2-plasma-treated, and (c) H_2-gas-treated UNCD films as the cathode.

H_2-plasma-treated UNCD films as cathodes (Figure 5b) and both of the devices using treated films as cathodes show better PI behavior than those using the pristine films as cathodes (Figure 5a). The PI characteristics of the plasma devices are better illustrated by the variation of the plasma current density (J_{pl}) versus E, which is plotted in Figure 4b. The microplasma devices based on the H_2-gas-treated UNCD films need 310 V (threshold field of (E_{th}) 0.31 V/μm, Figure 5c) to ignite the plasma, reaching a J_{pl} value of 0.54 mA/cm^2 at E_a = 0.55 V/μm (curve III, Figure 4b). In contrast, the microplasma devices based on H_2-plasma-treated UNCD films can be triggered at 330 V (E_{th} = 0.33 V/μm, Figure 5b) with J_{pl} = 0.50 mA/cm^2 (at E_a = 0.55 V/μm) (curve II, Figure 4b), whereas those based on pristine UNCD films required larger voltage of 350 V (E_{th} = 0.35 V/μm, Figure 5a) to trigger the plasma, with J_{pl} = 0.47 mA/cm^2 at E_a = 0.55 V/μm (curve I, Figure 4b). The values of E_{th} and J_{pl} are extracted from these figures and are also listed in Table 1, including the percentage of error in the measurements. The trend is similar to the change in EFE behavior (cf. Figure 4a). Restated, the best plasma illumination behavior, i.e., the lowest E_{th} value of 0.31 V/μm and the largest J_{pl} value of 0.54 mA/cm^2 at E_a = 0.55 V/μm, are observed for the microplasma devices based on H_2-gas-treated UNCD films.

In the meantime, we have estimated the plasma density (n_e) by using Child's law, shown in the following equation:[39]

$$n_e = \frac{J_c}{eu_B} \quad (1)$$

Here n_e is the electron density, J_c is the plasma current density at the cathode, e is the electron charge, and u_B is the Bhom velocity. The Bhom velocity of Ar ion strictly depends on the kinetic energy of the electron and the mass of the ion, which is described by the following equation:[40]

$$u_B = \sqrt{\frac{kT_e}{m_i}} \quad (2)$$

Here k is the Boltzmann constant and T_e is the electron temperature (7841 K).[41] By substituting the Bohm velocity in eq 1, we can obtain the complete equation for estimation of the electron density:

$$n_e = \frac{J_c\sqrt{m_i}}{e\sqrt{kT_e}} \quad (3)$$

By using the above formulas, we have obtained n_e versus E for H_2-gas-treated UNCD films (curve III, Figure 4c), achieving a value of $(n_e)_{III}$ = 2.46 × 10^{16}/m^3 at V = 500 V and a pressure of 2 Torr (266 Pa). Similarly, we have obtained an n_e value of 1.87 × 10^{16}/m^3 at V = 500 V for pristine diamond films (curve I, Figure 4c) and $(n_e)_{II}$ = 2.10 × 10^{16}/m^3 at V = 500 V for H_2-plasma-treated UNCD films (curve II, Figure 4c). These values are also listed in Table 1.

While the SEM micrographs and Raman spectra provide valuable information on the evolution of the surface morphology and bonding structure of the UNCD films due to H_2 post-treatment processes, how these processes modified the electric conductivity/EFE properties of the UNCD films is still not explained. This requires an investigation on the evolution of the UNCD's granular structure to understand the related mechanism. For this purpose, the samples were investigated using TEM and EELS (in TEM). It should be noted that when the samples were ion-milled only from the Si side, the TEM foil contained mostly the regions near the surface of the UNCD films, whereas when the samples were ion-milled both from the top and the bottom surfaces evenly at the same time, the thin foil contained the materials in the interior region of the UNCD films. The bright field (BF) and the associated dark field (DF) TEM micrographs for the surface region of the UNCD films are shown in Figure 6. Figure 6a$_I$

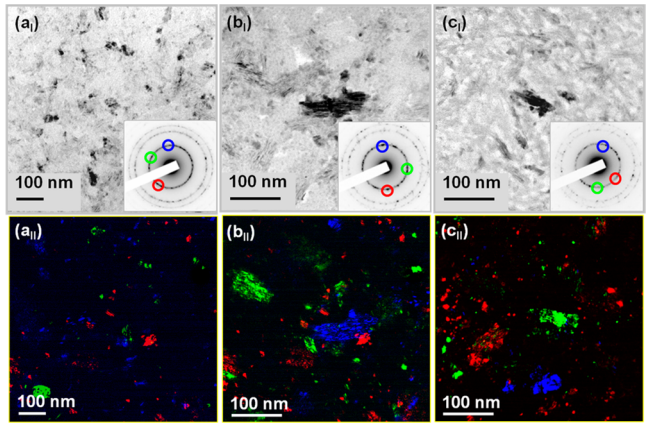

Figure 6. (a_I, b_I, c_I) Bright field and (a_{II}, b_{II}, c_{II}) composed dark field TEM micrographs of the surface regions of UNCD films (with the insets showing the SAED patterns). The samples were (a_I, a_{II}) pristine, (b_I, b_{II}) H_2-plasma-treated, and (c_I, c_{II}) H_2-gas-treated UNCD films.

shows that the surface region of the pristine UNCD films consists of ultrasmall spherical diamond grains (5−10 nm). The diffraction rings in the selected area electron diffraction (SAED) pattern (inset of Figure 6a$_I$) are smooth and continuous, indicating that the diamond grains are randomly oriented. The BF image shown in Figure 6b$_I$ indicates that, for the surface region of H_2-plasma-treated UNCD films, large diamond aggregates about hundreds of nanometer in size were induced and were evenly distributed among the matrix of ultrasmall grains, whereas Figure 6c$_I$ reveals that, for the surface region of H_2-gas-treated UNCD films, only a mild agglomeration process was induced, resulting in elongation of the diamond grains, which are around tens of nanometers in size. The SAED patterns of H_2-plasma- and H_2-gas-treated UNCD

films (insets of parts b_I and c_I, respectively, of Figure 6) contain spotty diffraction rings, implying again that these films contain some large diamond aggregates coexisting with the ultrasmall diamond grains. The size distribution of the diamond grains in these films is better illustrated by the composed dark field (c-DF) images, which are the superposition of several dark field images acquired using different diffraction spots (indicated in the inset SAED pattern). Parts a_{II}, b_{II}, and c_{II} of Figure 6 show the c-DF images of pristine, H_2-plasma-treated, and H_2-gas-treated UNCD films, corresponding to the BF images in parts a_I, b_I, and c_I, respectively, of Figure 6. These c-DF images indicate again that the H_2 plasma treatment process induced more marked coalescence of the ultrasmall diamond grains compared with the H_2 gas treatment process.

Figure 7 shows the TEM micrographs of the interior regions of the UNCD films, indicating that the interior region of all the

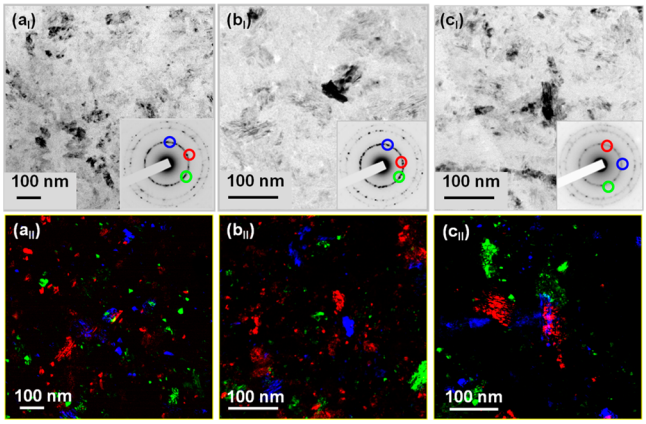

Figure 7. (a_I, b_I, c_I) Bright field and (a_{II}, b_{II}, c_{II}) composed dark field TEM micrographs of the interior regions of UNCD films (with the insets showing the SAED patterns). The samples were (a_I, a_{II}) pristine, (b_I, b_{II}) H_2-plasma-treated, and (c_I, c_{II}) H_2-gas-treated UNCD films.

films shows a granular structure similar to that observed in the surface region of the films (cf. Figure 6); i.e., there are large diamond aggregates distributed evenly among the matrix of nanosized diamond grains. However, more detailed examinations reveal a subtle difference in the microstructure of the interior region due to different H_2 post-treatment processes. While the interior region of the H_2-gas-treated UNCD films (Figure 7c_I) is very similar to the surface region, the interior region of the H_2-plasma-treated UNCD films (Figure 7b_I) contains smaller aggregates compared to the surface region. Again, the c-DF images were acquired to more clearly show the difference in granular structure of the interior regions of the UNCD films compared to the surface regions of the films as illustrated in Figure 7a_{II},b_{II},c_{II}, corresponding to the BF images in Figure 7a_I,b_I,c_I, respectively.

It should be pointed out that the H_2 plasma is much more aggressive in attacking the UNCD films as compared with the H_2 gas, since the H_2 plasma contains a large percentage of atomic hydrogen. However, due to the presence of sheath in the plasma, the plasma cannot penetrate deep into the diamond films; i.e., the interaction zone between the H_2 plasma and the UNCD films is very shallow. The H_2 plasma can not only attack the grain boundary phase but also etch the diamond grains.[42] Therefore, for "H_2 plasma" films, the UNCD films were treated in H_2 plasma for only 5 min, as a too long H_2 plasma treatment process might completely etch away the UNCD films. The simultaneous attack of the diamond grains and the grain boundaries will smooth out the surface roughness of the films. In contrast, the H_2 gas does not attack the diamond grains at all. Thus, the UNCD films were thermally heat-treated in a H_2 environment (1 atm) at 600 °C for 2 h for "H_2 gas" films. However, the H_2 gas can diffuse in and out of the UNCD films easily[43] and will interact with the grain boundary phase throughout the whole thickness of the UCND films. The preferential etching on the grain boundaries results in an increase in the roughness of the films.

The different behaviors in modifying the microstructure of the UNCD films due to H_2 plasma and H_2 gas post-treatment processes is interesting, but such information is still not able to account for the different degrees of improvement in the electrical conductivity/EFE properties of the UNCD films due to these processes. To understand the genuine mechanism of the enhancement of those properties, the bonding structure of the UNCD films was examined using EELS. Figure 8 shows the

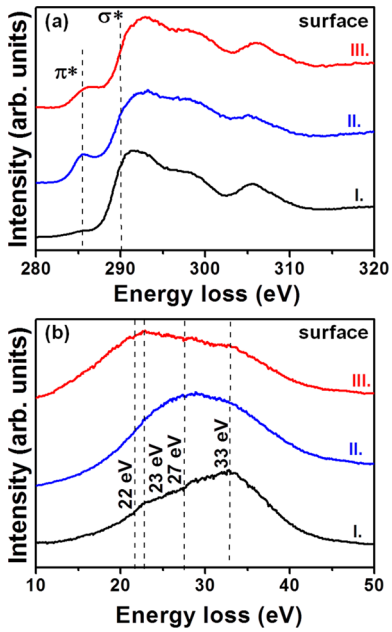

Figure 8. Selected area EELS spectra of the surface regions of UNCD films: (a) core-loss EELS spectra and (b) plasmon-loss EELS spectra of (I) pristine, (II) H_2-plasma-treated, and (III) H_2-gas-treated UNCD films corresponding to the TEM micrographs of Figure 6.

selected area EELS spectra corresponding to each micrograph in Figure 6, revealing that, in the surface region of the UNCD films, there are significant changes in the bonding structure due to the post-treatment processes. The carbon edge core-loss EELS spectra corresponding to these UNCD films (Figure 8a) indicate the presence of an abrupt rise near 289.5 eV (σ^* band) and a large dip in the vicinity of 302 eV, implying that the diamond nature of these materials was not altered due to the post-treatment processes.[44,45] Moreover, there is a prominent π^* band at 285.5 eV in core-loss EELS spectra for H_2-gas-treated (curve III, Figure 8a) and H_2-plasma-treated (curve II, Figure 8a) UNCD films, but this band is not visible in the spectra for pristine UNCD films (curve I, Figure 8a), indicating that a large proportion of sp^2-bonded carbon was induced, probably along the grain boundary regions of the UNCD films due to the H_2 gas and H_2 plasma post-treatment processes. However, it is still necessary to differentiate the nature of the

sp^2-bonded carbon to understand the genuine mechanism for enhancing the EFE/PI properties of the UNCD films due to these H_2 post-treatment processes. It should be pointed out that plasmon-loss EELS is the most effective measurement for distinguishing the crystalline sp^2-bonded carbons (the graphite) from the amorphous ones, as the plasmon-loss EELS spectrum for the graphitic phase shows a prominent peak at s_3 (27 eV) and that for the a-C phase shows a peak at s_1 (22 eV).[45,46] In contrast, the crystalline sp^3-bonded carbons, the diamond, show a peak due to the bulk plasmon at s_4 (33 eV) with a shoulder corresponding to the surface plasmon at s_2 (23 eV). The I_{s_2}/I_{s_4} ratio is about $1/\sqrt{2}$.

Figure 8b shows the plasmon-loss EELS spectra of the same regions. It is observed that the pristine UNCD films (curve I, Figure 8b) are dominated by s_2 and s_4 peaks, indicating that pristine UNCD films are diamond.[45] In contrast, the plasmon-loss EELS spectrum of H_2-plasma treated UNCD films (curve II, Figure 8b) is dominated by a larger s_3 band (~27 eV) with s_2 and s_4 bands of much smaller intensity, indicating that this region consists of some proportion of graphitic phases besides diamond. Quite the opposite, the plasmon-loss spectrum for H_2-gas-treated UNCD films (curve III, Figure 8b) is subjugated by an s_1 band (22 eV), in which s_2 and s_4 bands still dominate but with increased spectral weight of the s_1 band (22 eV). This result indicates that H_2 gas treatment induces a-C phases along with some graphitic phases in the UNCD films. From the four-probe measurements, it is observed that H_2 gas and H_2 plasma treatment processes resulted in similar low surface resistivity values (cf. Figure 3a) compared with those of the pristine UNCD films. Such a four-probe observation is in accord with the phenomena that both H_2 gas and H_2 plasma post-treatments induced the formation of a-C (and graphitic) phases on the surface region of the UNCD films.

In contrast, the four-probe measurements showed that H_2-gas-treated UNCD films possess a markedly lower through-film resistivity value than the H_2-plasma-treated UNCD films (cf. Figure 3b). The question now is how the H_2-gas-treated UNCD films show better through-film electrical conductivity/EFE properties than the H_2-plasma treated films. Apparently, an EELS analysis on the interior regions of the UNCD films is required to understand how the through-film conductivity was enhanced due to these H_2 post-treatment processes. The carbon edge core-loss EELS spectra (Figure 9a), corresponding to each TEM micrograph of Figure 7, indicate the presence of an abrupt rise near 290.5 eV (σ^* band) and a large dip in the vicinity of 302 eV for all the UNCD films, revealing that the diamond nature of the UNCD films was not altered for the interior region. However, it is interesting to observe that the prominent π^* band at 285.5 eV in the interior-loss EELS spectrum is observed only for H_2-gas-treated UNCD films (curve III, Figure 9a) and is not visible in the spectrum for either the pristine or the H_2-plasma-treated UNCD films (curves I and II, respectively, Figure 9a).

The plasmon-loss EELS spectra of the interior region of the UNCD films are shown in Figure 9b. The spectrum of the interior region of the pristine UNCD films (curve I, Figure 9b) shows behavior similar to that of the spectrum of the surface region in which s_2 and s_4 peaks are the dominant peaks, indicating that the pristine UNCD films are diamond.[45] There is no sp^2-bonded carbon in this region. Surprisingly, the plasmon-loss EELS spectrum of the interior region of the H_2-plasma-treated UNCD films (curve II, Figure 9b) also indicates

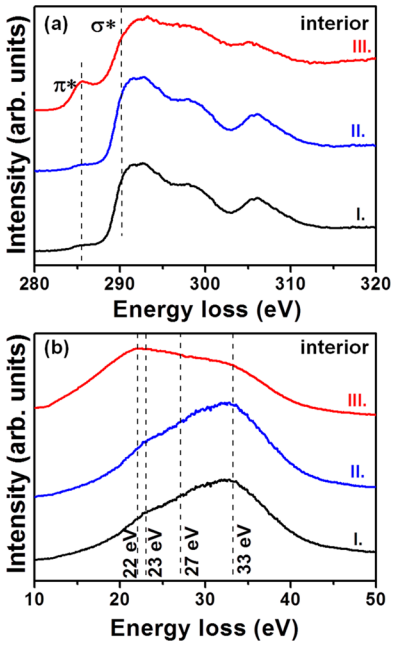

Figure 9. Selected area EELS spectra of the interior regions of UNCD films: (a) core-loss EELS spectra and (b) plasmon-loss EELS spectra of (I) pristine, (II) H_2-plasma-treated, and (III) H_2-gas-treated UNCD films corresponding to the TEM micrograph of Figure 7.

that s_2 and s_4 peaks are the dominant peaks, as for pristine UNCD films, with no presence of the s_3 band (~27 eV) of graphitic phases or s_1 band (~22 eV) of a-C phases, which is totally different from the case for the surface region of H_2-plasma-treated UNCD films (cf. curve II, Figure 8b). Here it is evident that H_2 plasma treatment induces the graphitic phases only in the surface region and not in the interior region of the UNCD films. In contrast, the plasmon-loss spectrum of the interior region of the H_2-gas-treated UNCD films (curve III, Figure 9b) shows that this region is still dominated by an s_1 band (22 eV) (including s_2 and s_4 bands of less intensity). Restated, the TEM−EELS analyses reveal that H_2 gas treatment induces a-C (and graphite) phases throughout the whole UNCD films, whereas the H_2 plasma treatment induces graphitic phases only at the surface region of the UNCD films.

Previous reports revealed that the a-C (or graphitic) phases are more conducting than the *t*-PA phases,[47,48] such that the formation of sp^2-bonded carbon phases at the grain boundaries creates conduction channels for the electrons to transport from the bottom side to the top side and emit to vacuum very easily. In this work, H_2 gas treatment induces a-C (or graphite) phases throughout the whole region of the UNCD films such that the electrons can be transported easily along the a-C (or graphite) phases at the grain boundaries throughout the diamond films to the emitting surface and are then emitted to vacuum without any difficulty as the diamond surfaces are NEA in nature.[49−51] On the contrary, for the H_2-plasma-treated UNCD films, the a-C (or graphitic) phases are present only at the surface region, and the interior region of these films remained essentially as diamond grains with lower amounts of a-C (or graphite) phases in the grain boundaries. This is the reason that the electrons cannot transport easily from the bottom side of the sample to the top side, resulting in inferior EFE properties. Consequently, the formation of a-C (or graphite) phases along the grain boundaries throughout the whole UNCD films due to H_2 gas treatment is the genuine reason for the enhanced EFE and PI

properties of these UNCD films. The formation of point defects seems not to be the source of enhancement of the EFE properties of H_2-treated UNCD films.

CONCLUSIONS

The effects of H_2 gas and H_2 plasma treatments on the structural and EFE properties of UNCD films were studied. The UNCD films were grown from an Ar/CH_4 gas mixture by an MPECVD system. To study the effects of bonding characteristics on the EFE properties, two different treatment methods were used. The first method was the H_2 plasma treatment, which was carried out in an MPECVD system at 600 °C. The second method was the H_2 gas treatment, which was done in the nonplasma quartz tube reactor connected with a H_2 gas supply line at 600 °C. We have observed that H_2-gas-treated UNCD films possess superior EFE properties compared to the H_2-plasma-treated UNCD films. TEM investigations revealed that the induction of a-C (or graphite) grain boundary phases in the whole region of the UNCD films due to H_2 gas treatment created conduction channels for the electrons to transport from the bottom to the top of the films and emit to vacuum very easily, resulting in the enhancement of EFE and PI properties. On the contrary, H_2 plasma treatment induced graphitic grain boundary phases only in the surface region of the UNCD films. The interior region is still mostly sp^3-diamond phases with lower amounts of a-C (or graphite) grain boundary phases, ensuing in inferior EFE and PI properties. As a consequence, the induction of a-C (or graphite) grain boundaries in the whole region of UNCD films due to H_2 gas treatment is the genuine factor for the enhancement of the EFE and the PI properties. The results support the potential use of UNCD films in a broad spectrum of applications in flat panel and microplasma display technologies.

AUTHOR INFORMATION

Corresponding Authors

*E-mail: nhtai@mx.nthu.edu.tw.
*E-mail: inanlin@mail.tku.edu.tw.

Notes

The authors declare no competing financial interest.

ACKNOWLEDGMENTS

The thank the National Science Council for financial support through Project Nos. NSC 101-2221-E-007-064-MY3 and NSC 102-2112-M-032-006.

REFERENCES

(1) Zuiker, C.; Krauss, A. R.; Gruen, D. M.; Pan, X.; Li, J. C.; Csencsits, R.; Erdemir, A.; Bindal, C.; Fenske, G. Physical and Tribological Properties of Diamond Films Grown in Argoncarbon Plasmas. *Thin Solid Films* **1995**, *270*, 154−159.

(2) Hupert, M.; Muck, A.; Wang, J.; Stotter, J.; Cvackova, Z.; Haymond, S.; Show, Y.; Swain, G. M. Conductive Diamond Thin-Films in Electrochemistry. *Diamond Relat. Mater.* **2003**, *12*, 1940−1949.

(3) Zhou, D.; Krauss, A. R.; Qin, L. C.; McCauley, T. G.; Gruen, D. M.; Corrigan, T. D.; Chang, R. P. H.; Gnaser, H. Synthesis and Electron Field Emission of Nanocrystalline Diamond Thin Films Grown from N_2/CH_4 Microwave Plasmas. *J. Appl. Phys.* **1997**, *82*, 4546−4550.

(4) Krauss, A. R.; Auciello, O.; Ding, M. Q.; Gruen, D. M.; Huang, Y.; Zhirnov, V. V.; Givargizov, E. I.; Breskin, A.; Chechen, R.; Shefer, E.; Konov, V.; Pimenov, S.; Karabutov, A.; Rakhimov, A.; Suetin, N. Electron Field Emission of Ultrananocrystalline Diamond Films. *J. Appl. Phys.* **2001**, *89*, 2958−2967.

(5) Sharda, T.; Rahaman, M. M.; Nukaya, Y.; Soga, T.; Jimbo, T.; Umeno, M. Structural and Optical Properties of Diamond and Nano-Diamond Films Grown by Microwave Plasma Chemical Vapor Deposition. *Diamond Relat. Mater.* **2001**, *10*, 561−567.

(6) Williams, O. A.; Curat, S.; Gerbi, J. E.; Gruen, D. M.; Jackman, R. B. n-Type Conductivity in Ultrananocrystalline Diamond Films. *Appl. Phys. Lett.* **2004**, *85*, 1680−1682.

(7) Sankaran, K. J.; Joseph, P. T.; Chen, H. C.; Tai, N. H.; Lin, I. N. Investigation in the Role of Hydrogen on the Properties of Diamond Films Grown Using $Ar/H_2/CH_4$ Microwave Plasma. *Diamond Relat. Mater.* **2011**, *20*, 232−237.

(8) Sankaran, K. J.; Kumar, N.; Kurian, J.; Ramadoss, R.; Chen, H. C.; Tyagi, A. K.; Dash, S.; Lee, C. Y.; Tai, N. H.; Lin, I. N. Improvement in Tribological Properties by Modification of Grain Boundary and Microstructure of Ultrananocrystalline Diamond Films. *ACS Appl. Mater. Interfaces* **2013**, *5*, 3614−3624.

(9) Zhu, W.; Kochanski, G. P.; Jin, S. Low-Field Electron Emission from Undoped Nanostructured Diamond. *Science* **1998**, *282*, 1471−1473.

(10) Cheng, H. F.; Horng, C. C.; Chiang, H. Y.; Chen, H. C.; Lin, I. N. Modification on the Microstructure of Ultrananocrystalline Diamond Films for Enhancing Their Electron Field Emission Properties via a Two-Step Microwave Plasma Enhanced Chemical Vapor Deposition Process. *J. Phys. Chem. C* **2011**, *115*, 13894−13900.

(11) Teng, K. Y.; Huang, P. C.; Shih, W. C.; Lin, I. N. The Induction of a Graphitic-like Phase by Fe-Coating/Post-Annealing Process To Improve the Electron Field Emission Properties of Ultrananocrystalline Diamond Films. *Diamond Relat. Mater.* **2012**, *24*, 188−194.

(12) Lin, I. N.; Chen, Y. H.; Cheng, H. F. Modification of Emission Properties of Diamond Films Due to Surface Treatment Process. *Diamond Relat. Mater.* **2000**, *9*, 1574−1581.

(13) Nebel, C. E. Surface-Conducting Diamond. *Science* **2007**, *318*, 1391−1392.

(14) Seshan, V.; Ullien, D.; Castellanos-Gomez, A.; Sachdeva, S.; Murthy, D. H. K.; Savenije, T. J.; Ahmad, H. A.; Nunney, T. S.; Janssens, S. D.; Haenen, K.; Nesládek, M.; van der Zant, H. S. J.; Sudhölter, E. J. R.; de Smet, L. C. P. M. Hydrogen Termination of CVD Diamond Films by High-Temperature Annealing at Atmospheric Pressure. *J. Chem. Phys.* **2013**, *138*, 234707.

(15) Wang, M.; Simon, N.; Decorse-Pascanut, C.; Bouttemy, M.; Etcheberry, A.; Li, M. S.; Boukherroub, R.; Szunerits, S. Comparison of the Chemical Composition of Boron-Doped Diamond Surfaces upon Different Oxidation Processes. *Electrochim. Acta* **2009**, *54*, 5818−5824.

(16) Ristein, J. Surface Science of Diamond: Familiar and Amazing. *Surf. Sci.* **2006**, *600*, 3677−3689.

(17) Ariano, P.; Baldelli, P.; Carbone, E.; Gilardino, A.; Lo Guidice, A.; Lovisolo, D.; Manfredotti, C.; Novara, M.; Sternschulte, H.; Vittone, E. Cellular Adhesion and Neuronal Excitability on Functionalised Diamond Surfaces. *Diamond Relat. Mater.* **2005**, *14*, 669−674.

(18) Tachiki, M.; Kaibara, Y.; Sumikawa, Y.; Shigeno, M.; Banno, T.; Song, K. S.; Umezawa, H.; Kawarada, H. Diamond Nanofabrication and Characterization of Biosensing Applications. *Phys. Status Solidi A* **2003**, *199*, 39−43.

(19) Nebel, C. E.; Kato, H.; Rezek, B.; Shin, D.; Takeuchi, D.; Watanabe, H.; Yamamoto, T. Electrochemical Properties of Undoped Hydrogen Terminated CVD Diamond. *Diamond. Relat. Mater.* **2006**, *15*, 264−268.

(20) Lafosse, A.; Berlin, M.; Michaelson, S.; Azria, R.; Akhvlediani, R.; Hoffmann, A. Surface Defects Induced by In-Situ Annealing of Hydrogenated Polycrystalline Diamond Studied by High Resolution Electron Energy Loss Spectroscopy. *Diamond Relat. Mater.* **2008**, *17*, 949−953.

(21) Kawarada, H. Hydrogen-Terminated Diamond Surface and Interfaces. *Surf. Sci. Rep.* **1996**, *26*, 205−259.

(22) Hoffmann, R.; Kriele, A.; Obloh, H.; Hees, J.; Wolfer, M.; Smirnov, W.; Yang, N.; Nebel, C. E. Electrochemical Hydrogen

Termination of Boron-Doped Diamond. *Appl. Phys. Lett.* **2010**, *97*, 052103.
(23) Manfredotti, Ch.; Bonino, P.; Pierre, M. D. L.; Vittone, E.; Manfredotti, C. About Orientation Dependence of Physico-Chemical Properties of HPHT Diamond Surface Thermally Treated in H_2 and D_2 Environments. *Diamond Relat. Mater.* **2010**, *19*, 279−283.
(24) Ando, T.; Ishii, M.; Kamo, M.; Sato, Y. Thermal Hydrogenation of Diamond Surfaces Studied by Diffuse Reflectance Fourier-Transform Infrared, Temperature-Programmed Desorption and Laser Raman Spectroscopy. *J. Chem. Soc., Faraday Trans.* **1993**, *89*, 1783−1789.
(25) Fizzotti, F.; Lo Giudice, A.; Manfredotti, C.; Manfredotti, C.; Castellino, M.; Vittone, E. Diamond Surface Conductivity after Exposure to Molecular Hydrogen. *Diamond Relat. Mater.* **2007**, *16*, 836−839.
(26) Dong, C. L.; Chen, S. S.; Chiou, J. W.; Chen, Y. Y.; Guo, J. H.; Cheng, H. F.; Lin, I. N.; Chang, C. L. Effect of Surface Treatments on the Electronic Properties of Ultra-Nanocrystalline Diamond Films. *Diamond Relat. Mater.* **2008**, *17*, 1150−1153.
(27) Lee, Y. C.; Pradhan, D.; Lin, S. J.; Chia, C. T.; Cheng, H. F.; Lin, I. N. Effect of Surface Treatment on the Electron Field Emission Property of Nano-Diamond Films. *Diamond Relat. Mater.* **2005**, *14*, 2055−2058.
(28) Panda, K.; Sankaran, K. J.; Panigrahi, B. K.; Tai, N. H.; Lin, I. N. Direct Observation and Mechanism for Enhanced Electron Emission in Hydrogen Plasma-Treated Diamond Nanowire Films. *ACS Appl. Mater. Interfaces* **2014**, *6*, 8531−8541.
(29) Fowler, R. H.; Nordheim, L. Electron Emission in Intense Electric Fields. *Proc. R. Soc. London, Ser. A* **1928**, *119*, 173−181.
(30) Ferrari, A. C.; Robertson, J. Origin of the 1150 cm^{-1} Raman Mode in Nanocrystalline Diamond. *Phys. Rev. B* **2001**, *63*, 121405.
(31) Corrigan, T. D.; Gruen, D. M.; Krauss, A. R.; Zapol, P.; Chang, R. P. H. The Effect of Nitrogen Addition to Ar/CH4 Plasmas on the Growth, Morphology and Field Emission of Ultrananocrystalline Diamond. *Diamond Relat. Mater.* **2002**, *11*, 43−48.
(32) Ferrari, A. C.; Robertson, J. Interpretation of Raman Spectra of Disordered and Amorphous Carbon. *Phys. Rev. B* **2000**, *61*, 14095−14107.
(33) Kalish, R. Doping of Diamond. *Carbon* **1999**, *37*, 781−785.
(34) Heng, H.; Jun, H. X.; Wen, B. B.; Hu, C. X. Effects of Annealing Time on the Microstructural and Electrochemical Properties of B-Doped Nanocrystalline Diamond Films. *Acta Phys. Sin.* **2012**, *61*, 148101.
(35) Tsai, W. C.; Wang, S. J.; Chang, C. L.; Chen, C. H.; Ko, R. M.; Liou, B. W. Improvement of Field Emission Characteristics of Tungsten Oxide Nanowires by Hydrogen Plasma Treatment. *EPL* **2008**, *84*, No. 16001.
(36) You, J. B.; Zhang, X. W.; Cai, P. F.; Dong, J. J.; Gao, Y.; Yin, Z. G.; Chen, N. F.; Wang, R. Z.; Yan, H. Enhancement of Field Emission of the ZnO Film by the Reduced Work Function and the Increased Conductivity via Hydrogen Plasma Treatment. *Appl. Phys. Lett.* **2009**, *94*, 262105.
(37) Zheng, Z.; Liao, L.; Yan, B.; Zhang, J. X.; Gong, H.; Shen, Z. X.; Yu, T. Enhanced Field Emission from Argon Plasma-Treated Ultra-Sharp α-Fe_2O_3 Nanoflakes. *Nanoscale Res. Lett.* **2009**, *4*, 1115−1119.
(38) Robertson, J. Mechanism of Electron Field Emission from Diamond and Diamond-Like Carbon. *IVMC 98*, Asheville, NC, July 19−24, 1998; IEEE: Piscataway, NJ, 1998; pp 162−163.
(39) Lieberman, M. A.; Lichtenberg, A. J. *Principles of Plasma Discharges and Materials Processing*, 2nd ed.; John Wiley & Sons: Hoboken, NJ, 2005.
(40) Chapman, B. *Sputtering and Plasma Etching*; John Wiley & Sons: New York, 1980.
(41) Srinivasu, K.; Sankaran, K. J.; Leou, K. C.; Tai, N. H.; Lin, I. N. Microplasma Device Architectures with Various Diamond Nanostructures and Their Characteristics. *Plasma Sources Sci. Technol.* **2014**, submitted for publication.
(42) Villalpando, I.; John, P.; Porro, S.; Wilson, J. I. B. Hydrogen Plasma Etching of Diamond Films Deposited on Graphite. *Diamond Relat. Mater.* **2011**, *20*, 711−716.
(43) Joseph, P. T.; Tai, N. H.; Lee, C. Y.; Niu, H.; Pong, W. F.; Lin, I. N. Field Emission Enhancement in Nitrogen-Ion-Implanted Ultrananocrystalline Diamond Films. *J. Appl. Phys.* **2008**, *103*, 043720.
(44) Gruen, D. M.; Liu, S.; Krauss, A. R.; Luo, J.; Pan, X. Fullerenes as Precursors for Diamond Film Growth without Hydrogen or Oxygen Additions. *Appl. Phys. Lett.* **1994**, *64* (12), 1502−1504.
(45) Kovarik, P.; Bourdon, E. B. D.; Prince, R. H. Electron-Energy-Loss Characterization of Laser-Deposited *a*-C, *a*-C:H, and Diamond Films. *Phys. Rev. B* **1993**, *48*, 12123−12129.
(46) Prawer, S.; Peng, J. L.; Orwa, J. O.; McCallum, J. C.; Jamieson, D. N.; Bursill, L. A. Size Dependence of Structural Stability in Nanocrystalline Diamond. *Phys. Rev. B* **2000**, *62*, R16360−R16363.
(47) Sankaran, K. J.; Kurian, J.; Chen, H. C.; Dong, C. L.; Lee, C. Y.; Tai, N. H.; Lin, I. N. Origin of a Needle-like Granular Structure for Ultrananocrystalline Diamond Films Grown in a N_2/CH_4 plasma. *J. Phys. D: Appl. Phys.* **2012**, *45*, 365303.
(48) Teng, K. Y.; Chen, H. C.; Chiang, H. Y.; Horng, C. C.; Cheng, H. F.; Sankaran, K. J.; Tai, N. H.; Lee, C. Y.; Lin, I. N. The Role of Nano-Graphite Phase on the Enhancement of Electron Field Emission Properties of Ultrananocrystalline Diamond Films. *Diamond Relat. Mater.* **2012**, *24*, 126−133.
(49) Yamaguchi, H.; Masuzawa, T.; Nozue, S.; Kudo, Y.; Saito, I.; Koe, J.; Kudo, M.; Yamada, T.; Takakuwa, Y.; Okano, K. Electron Emission from Conduction Band of Diamond with Negative Electron Affinity. *Phys. Rev. B* **2009**, *80*, 165321.
(50) Geis, M. W.; Deneault, S.; Krohn, K. E.; Marchant, M.; Lyszczarz, T. M.; Cooke, D. L. Field Emission at 10 Vcm^{-1} with Surface Emission Cathodes on Negative-Electron-Affinity Insulators. *Appl. Phys. Lett.* **2005**, *87*, 192115.
(51) Cui, J. B.; Stammler, M.; Ristein, J.; Ley, L. Role of Hydrogen on Field Emission from Chemical Vapor Deposited Diamond and Nanocrystalline Diamond Powder. *J. Appl. Phys.* **2000**, *88*, 3667−3673.